

TALKING WITH THE LATENTS - HOW TO CONVERT YOUR LLM INTO AN ASTRONOMER

Ilay Kamai

Department of Physics

Technion - Israel Institute of Technology

Haifa, 32000, Israel

ilay.kamai@campus.technion.ac.il

Marc-Huertas Company

Instituto de Astrofísica de Canarias

E-38205 La Laguna, Tenerife, Spain

Michael J. Smith

Center for Astrophysics, Harvard & Smithsonian

60 Garden St. Cambridge, MA 02138, USA

Hagai B. Perets

Technion - Israel Institute of Technology

Haifa, 32000, Israel

ABSTRACT

Recent advances in Large Language Models (LLMs) offer unique opportunities for scientific tasks, yet their ability to reason over complex numerical data remains largely unexplored. We propose a simple mechanism to introduce domain-specific physical knowledge into LLMs by fusing pre-trained latent physical features with a pre-trained language model.

Our method employs a teacher-student knowledge distillation framework where a large LLM (teacher) generates synthetic question-answer supervision to transfer physical reasoning to a smaller LLM (student). The student is conditioned on latent physical features and trained via a lightweight adapter and Low-Rank Adaptation (LoRA). We demonstrate that this approach, applied to models with 1B, 8B, and 32B parameters, enables effective reasoning over real scientific data. Our models substantially outperform strong baselines, such as Gemini 3 Pro, across multiple downstream tasks without task-specific fine-tuning. We show that the model combines latent information with general physical understanding to predict complex properties and can be "steered" by identifying physically meaningful directions in the latent space. This allows for explicit physical manipulation and natural language interpretation of latent structures. While our experiments focus on astrophysics, the framework is domain-agnostic and applicable to various scientific fields. Our main contribution is a general framework for using LLMs as interpretable interfaces to scientific latent spaces, enabling a single model to perform diverse tasks through natural language guidance. This work marks a step toward developing scientifically capable and useful LLMs.

1 INTRODUCTION

The integration of Large Language Models (LLMs) into the scientific workflow marks a paradigm shift in how researchers interface with information. While these models have demonstrated remarkable proficiency in some scientific tasks, their utility remains largely confined to the textual and visual domains. A critical frontier in "AI for Science" is the transition from processing scientific text to reasoning directly over the numerical and physical data that defines scientific discovery. Despite their sophistication, standard LLM architectures often struggle with numerical reasoning (Rahman & Mishra, 2025), creating a gap between natural language and empirical data.

Motivation. The main motivation of this work is the need to combine physics foundation models and LLMs in a scientifically useful manner. Each one of them has unique advantages, and the potential for knowledge alignment between them has far-reaching outcomes. One of them is interpretability: since LLMs understand both natural language and high-dimensional data, they can serve as a 'bridge' between humans and machine learning representations, which are usually hard to interpret. Another possible benefit from such a combination is a flexible downstream task: currently,

scientific foundation models serve as a backbone for different downstream tasks. However, each task requires a specific downstream head and training. Using an LLMs as a ‘lingua franca’ interface enables a more flexible downstream behavior, driven by natural language, and encapsulated in a single model.

Methodology. In this work, we develop a general framework to combine scientific foundation models and LLMs. The scientific domain we chose to focus on is astrophysics, but nothing is specific to astrophysics in our method, and it can be transferred to other scientific domains with dedicated machine learning models. As this is one of the first steps towards a language-astronomy multimodal model (other than astronomical images), we chose a simple early fusion approach, where we project the astronomical latent features into the token embedding space of the LLM using an MLP, which we refer to as the Adapter Network (AN). Therefore, the full model is a language model with additional effective tokens resulting from the AN. As such, it is straightforward to generate text conditioned on latent features.

2 RELATED WORK

Advances in LLMs have already had a wide-ranging impact on how we do science. LLM agents can now review and write scientific papers (Villaescusa-Navarro et al., 2025; Zhuang et al., 2025), and even act as a ‘virtual lab’ that suggests and implements novel research ideas (Swanson et al., 2025). However, these agents typically access scientific data indirectly by writing code to an external tool (e.g., ESM, AlphaFold-multimer). This resonates with the known limitations of current LLMs with numerical data (Rahman & Mishra, 2025) and the gap in performance between theoretical questions and data analysis (Carrit Delgado Pinheiro et al., 2025). On the other hand, scientific foundation models become popular in many scientific fields and show strong performance across domains (e.g., Leung & Bovy, 2024; Parker et al., 2025; Smith et al., 2024; Euclid Collaboration et al., 2025; Bardhan et al., 2025; Hayes et al., 2025; Bodnar et al., 2025; Abramson et al., 2024). Notably however, those models do not use natural language as a modality. As a consequence, there is currently a clear distinction between scientific foundational models and LLMs. The idea of a scientific-LLM usually refers to the injection of scientific knowledge into existing LLMs using various methods (for review, see Hu et al. (2025) and Eger et al. (2025)). However, most works in the field of scientific-LLM focus on fine-tuning LLM on high-quality textual and visual data to create improved reasoning (Xie et al., 2023; Bai et al., 2025; Cherian et al., 2024), object descriptions (Mishra-Sharma et al., 2024), search engines (Koblischke et al., 2025), and scientific chatbots (Zaman et al., 2025). While such models often achieve impressive results compared to general LLMs (de Haan et al., 2025), they are usually focused on two specific modalities—text and images. While those modalities are very useful for different scientific tasks, real scientific research has a much larger modality landscape, and the combination of such modalities with LLMs for real scientific tasks is still largely unexplored. Our approach differs from the above by directly aligning the latent space of a scientific model with the LLM. This fusion is motivated by methods that project latent features into token space to improve interpretability (e.g., Tennenholz et al., 2023), treating the output of the scientific encoder as effective tokens for the language model.

3 QUESTION-ANSWER DATASET

In this section, we describe the dataset used in our experiments. Our dataset consists of astronomical latent features that are the output of a stellar spectra foundation model, and a textual description of the same samples. In this work, we use two different spectra foundation models. The first model is a pretrained spectra encoder from Kamai et al. (2025). In their paper, the authors presented a multimodal model for stellar spectra and light curves, which consists of two separate encoders, a spectra encoder and a light curve encoder, and an alignment module. For this work, we utilized the spectra encoder, which comprises a CNN encoder-decoder enhanced with a Conformer module (Gulati et al., 2020) that processes the averaged bottleneck from the CNN encoder and yields stellar predictions. We therefore refer to this model as *Spectral Conformer (SC)*. The SC model was trained on approximately 5 million spectroscopic measurements from the LAMOST survey (Zhao et al., 2012), with two objectives—a self-supervised masked reconstruction and a supervised prediction of stellar parameters—temperature (T_{eff}), surface gravity ($logg$), and metallicity (FeH). The second model, which we use in section 5.3, use the same input but with a slightly different architecture - it

first divides the masked spectra into patches, using a 1D-CNN, and then process it with a transformer encoder. The resulting latent tokens are sent into an MLP decoder, which produces clean spectra, and an MLP regressor that predicts stellar parameters. We refer to this model as *Spectral ViT* (SViT). The SViT model was trained on the same dataset and with the same objectives. The resulting features, from both SC and SViT models, are of dimension 2048. To construct the textual description, we used the stellar parameters, as given by the LAMOST stellar parameter pipeline (LASP) (Wu et al., 2014), and generated a short question-answer pair for this specific star. The question-answer pair was generated by prompting Gemini 2.5 flash with the stellar information and asking it to describe the star as a professional astronomer with no more than 50 words. In addition, to enable the fusion of latent features into the input, we added K empty tokens at the beginning of the question that were used as placeholders for the latent features. As a compromise between performance and compute, we chose $K = 8$. Finally, to further improve the diversity of the dataset, we randomly add a follow-up question for 70% of the samples about the stellar type of the star. The follow-up question includes all the previous context, and the answer to the follow-up question includes only the stellar type without further description. The total size of the dataset consisted of 40,000 samples, which were split into training (80%), validation (10%), and test datasets (10%). An example of a dataset sample is shown in Figure 1.

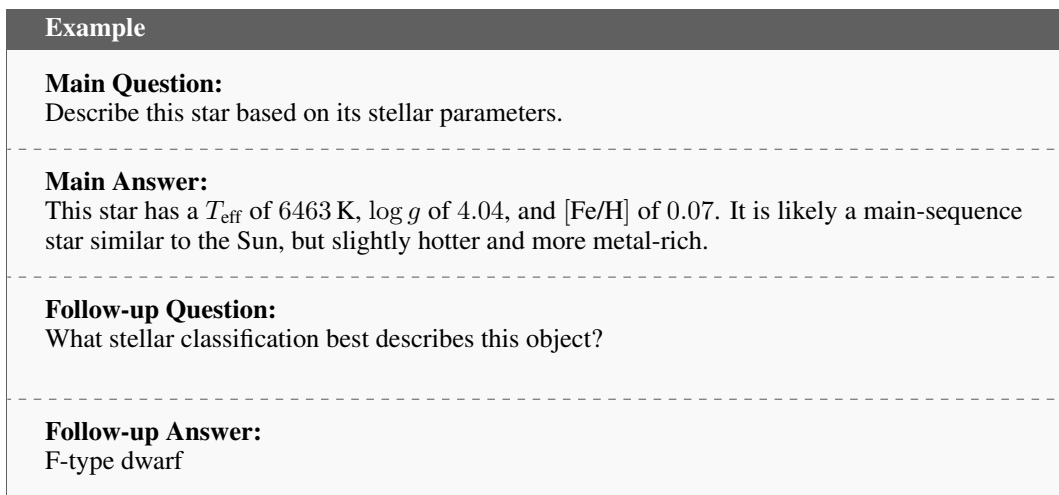


Figure 1: An example of our question-answer dataset. The follow-up questions are added randomly in 70% of the cases.

4 LATENT INTERPETER MODEL

Our model, which we call *Latent Interpreter* (LI), consists of a simple composition of a pre-trained LLM and a pre-trained spectra model. The input of the LLM is the question tokens as described in section 3. They are embedded in a high-dimensional space using the existing token encoder of the LLM. The input of the spectra model is the corresponding spectra. Masked spectra are processed by the spectra model (SC or SViT), resulting in latent features. Features are further transformed into effective token embeddings using a dedicated *Adapter Network* (AN). The AN projects the latent features into K tokens with the same dimensions as the token embedding space. The resulting K effective tokens are concatenated to the original token embeddings and sent into the next LLM layers. This simple fusion is motivated by Tennenholz et al. (2023), which suggested a similar approach to improve latent space interpretability for LLMs. Training is done in two steps—first, only the AN is trained for several epochs. Next, the AN is frozen, and we finetune the LLM with a low-rank adaptation (LoRA) (Hu et al., 2021). This strict distinction between training the AN and finetuning the LLM is crucial since a good transformation of the latent features into the LLM embedding needs to be learned before we can effectively fine-tune the LLM. A diagram of the model is shown in Figure 2.

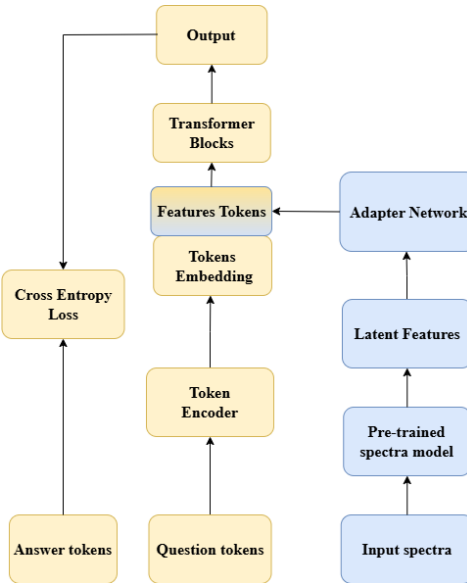


Figure 2: High-level diagram of the Latent Interpreter model. Blue colors represent the spectra model. Yellow colors represent the LLM.

5 EXPERIMENTAL RESULTS

The following subsections discuss our general findings.

5.1 EFFECT OF LLM SIZE

Learning local concepts. First, we want to test the ability to infer correct physical information. For that, we train three models, each one using a different pre-trained LLM—Llama-1B, Llama-8B, and Qwen-32B. For the latent features, we used the SC model. The latent features in this case were taken as the output of the Conformer block. All the models were trained with an identical dataset and hyperparameters. After training, we test the models on a separate test set, extract the values of the stellar parameters ($Teff$, $logg$, FeH) from the generated text, and compare them with the ground truth values. Besides being the most basic stellar parameters to infer from spectra, those parameters were also part of the original training of the SC model. Therefore, we expect strong alignment between latent features and the stellar parameters values, and as a consequence, we call them *local concepts* as they are represented entirely by the latent space. Using this definition, the first experiment tests the ability of the LLM to extract the information stored in specific latent features using the AN. To compare our method with baselines, we use two additional models. First, we use the results of the SC model from Kamai et al. (2025). We refer to this model as our *spectra baseline model*. Second, we use the Gemini 3 pro model (preview release). To test its ability to infer stellar parameters, we provide it with the following information: arrays of the measured wavelengths and flux, and an image that shows a plot of the wavelength vs. flux. In addition, we provide it with a general context in the form of short guidelines for stellar spectra analysis, which was created using Gemini 3 pro’s deep research feature (approximately 40 000 tokens). The prompt asks the model to act as a professional astrophysicist and to analyze the spectrum using all the given information. We refer to this model as *Gemini baseline model*.

Table 1 compares the performance between our three trained models, tested on 100 samples, the spectra baseline model, and the Gemini baseline model, tested on 50 samples, for efficiency. We measure the median absolute error (MedAE), and the root mean squared error (RMSE), which is more sensitive to outliers. We see that the Gemini baseline model performs much worse than all the trained models. In addition, our trained models achieve comparable or better results compared to those of the spectra baseline model, with no one model performing consistently better than the others. The immediate conclusion is that all three models were able to effectively extract information from local concepts stored in the latent features, much better than a state-of-the-art LLM that uses

general knowledge and a multimodal input (Gemini baseline model). The comparison to a state-of-the-art (SOTA) LLM is, of course, not fair from a data perspective—the SOTA LLM didn’t see the specific latent features but only the raw data. However, the purpose of such a comparison is to convince that for scientific tasks related to specific data, general pre-training is not sufficient, even for SOTA LLMs, and that our special training approach is required.

Table 1: Performance comparison for T_{eff} , $\log g$ and metallicity (Fe/H). All values were extracted from the models’ answers.

Model	T_{eff} [K]		$\log g$ [dex]		[Fe/H] [dex]	
	MedAE ↓	RMSE ↓	MedAE ↓	RMSE ↓	MedAE ↓	RMSE ↓
LI-Llama-1B	30.31	114.64	0.04	0.19	0.04	0.14
LI-Llama-8B	26.50	63.96	0.04	0.11	0.03	0.06
LI-Qwen-32B	23.05	112.07	0.03	0.13	0.05	0.53
Spectra Baseline model	35.58	85.18	0.05	0.12	0.03	0.06
Gemini 3 Pro (Zero-Shot)	357.70	564.97	0.28	0.75	0.15	0.22

Learning global concepts. Next, we want to test if the models can combine information from latent features with their own general physical knowledge. For that, we perform a similar experiment as used to infer basic stellar parameters, but we also test the performance on three follow-up questions. First, we tested the prediction of the spectral type of the star. In addition to spectral type, which appeared in the training, we also test the performance on two additional follow-up questions that the model was not trained on—we provide the model with the radius of the star and ask it to predict the luminosity and mass of the star. The values of the radius, luminosity, and mass were taken from Berger et al. (2020). All three tasks require combined information - inferring the spectral type requires a combination of T_{eff} and $\log g$. Calculating mass and luminosity from the radius alone is not possible, and requires knowledge about T_{eff} and $\log g$ (specific knowledge) as well as the analytical relationships between the parameters (general knowledge). Therefore, these questions test whether the models can combine the local concepts with general knowledge that comes from general pre-training. Table 2 shows the results. Here, we observe a more consistent trend: the largest model (Qwen-32B) performs best across all tasks, with the exception of the luminosity RMSE. Given that the MedAE of Qwen-32B remains better than other models, we conclude that the higher RMSE is driven primarily by a greater number of outliers for this model. This experiment highlights a capability unique to the LLM architecture: multimodal reasoning. To predict luminosity or mass, the model must fuse information from three distinct sources: the specific spectral data stored in the latent features (T_{eff}), the auxiliary data provided via the text prompt (Radius), and the general physical laws stored in the LLM’s weights (e.g., Stefan-Boltzmann law). A standard regression head trained on spectral features would fail this task, as it lacks access to the auxiliary text input (Radius), while a regular LLM would fail, as it lacks access to the spectral data. By combining text and numerical features, our model can perform zero-shot inference on these tasks.

Table 2: Performance comparison for luminosity, mass, and spectral type.

Model	L [L_{\odot}]		M [M_{\odot}]		Spectral Type Acc.
	MedAE ↓	RMSE ↓	MedAE ↓	RMSE ↓	
LI-Llama-1B	4.54	62.24	0.73	6.48	17.3%
LI-Llama-8B	5.62	109.15	1.08	3.21	37.4%
LI-Qwen-32B	2.53	70.36	0.38	1.58	47.5%

The fact that, for all the global concepts, the best performance was achieved by the largest model (Qwen-32B), implies that increasing the LLM size should improve the flexibility of the final model and enable answering more complex questions without dedicated training.

5.2 CAUSAL CONTROL

Next, we want to test if we can steer the model’s output in a controllable and physical way. To test this, we conduct a steering experiment. Here, we are largely following the procedure suggested in Alexa Fear et al. (2025)—first, we identify ‘concept directions’ in the features’ latent space of the SC model. To identify such a direction, we collect samples from the training set that obey a constraint defined by some physical concept (for example, $T_{eff} > 6000$ K for a ‘hot star’), and average all their latent features to get an average representation of a concept. We then repeat the process with the opposite concept (for example, $T_{eff} < 4250$ K for ‘cool star’), and we subtract the two averages to get the direction of the concept in latent space. We then use this direction as a steering vector—during inference, we add this direction to the original latent features. Specifically, given a latent feature, f , and a direction feature f_{direc} , the final features given to the model are $f' = f + \alpha \frac{f_{direc}}{\|f_{direc}\|^2}$, where α controls the steering strength. For each sample, we tested different concepts and changed α between -2 and 2 . To interpret the results, we extract the physical parameters from the generated answer and plot them in T_{eff} — $\log g$ space. Figure 3 shows an example of steering with two different concepts—stellar evolution concept (dwarfs to giants) and stellar age concept (young to old). The evolution concept was derived from Ciardi et al. (2011), which presented a criterion to identify giants based on T_{eff} and $\log g$ cuts. We took all the samples that matched the criterion as giants and all others as dwarfs. This is, of course, a crude estimation as the evolution of stars is continuous and includes a ‘sub-giant’ regime. For the age concept, we used isochrone ages from Berger et al. (2020). We took samples with ages younger than the 25^{th} percentile as ‘young’ and samples with ages older than the 75^{th} percentile as ‘old’. This is again a rough estimation, as isochrone ages are accurate only at certain evolutionary phases (main sequence turn off, for example). In other phases, isochrones are densely packed, and the derived age can have very large errors. Since we focused on the ability to steer the model, and not on the effect of LLM size, in this experiment, we used only Llama-8B LLM. We can see that the effect of steering matches our physical understanding—when the model is steered towards a dwarf or a giant (left panel), it moves in the right direction, almost perpendicular to the black dashed line. When it steered with age direction, the model again moves in the expected direction (bluer circles move toward magenta isochrones), this time more perpendicular to the isochrones, as expected. In both cases, the full steering paths reside in a physical region, where the population of real stars is large. One example of that is in the right panel; when $\alpha = -1$, the parameters sit on the edge of the gray background, and we see that for the next point, $\alpha = -2$, we have a big ‘jump’ in parameters, much bigger compared to previous steps, to avoid the non-physical area. We observed that our model produced more physical trajectories compared to an MLP that was trained to predict stellar parameters from spectral features, and was steered in the same way (see Appendix A.3). It is also important to emphasize that steering changes the entire generated answer and not only the extracted parameters. For example, when the model is steered towards a dwarf star, the entire description would be of a dwarf (see, for example, Figure 4). We tested additional concepts — hot to cool, low $\log g$ to high $\log g$, metal poor to metal rich, and low mass to high mass. In all cases, we see the same physically-consistent behavior (see Appendix A.3).

5.3 EFFECT OF LATENT DIMENSION

In section 5.1, we tested the effect of changing the LLM size with fixed latent space. Now we investigate the opposite direction and ask how the structure and characteristics of the latent space affect the final results, given a fixed-size LLM. To test this, we used the SViT model as described in section 3. The final features of the SViT model were taken to be the classification token that was used to predict stellar parameters. While the features from the SC model are sparse (approximately 60% of the elements are $< 10^{-30}$), the features from the SViT model are dense. Figure 5 shows a statistical comparison between the sparse and dense features. An important point to emphasize is that both features have the same dimensionality (2048), and that both networks show similar performance on stellar parameters prediction.

We trained two models with a Llama-8B LLM, each one with different latent features. Training of both models was identical, except for the latent features given to the LLM. Table 3 shows the results of basic parameter prediction (local concepts). We see a huge gap in performance between the different features. Using the same intuition as in section 5.1 that the basic features represent specific knowledge which gained only during our training, this striking difference between the models implies that sparsity is crucial for the successful interpretation of features as effective tokens. While

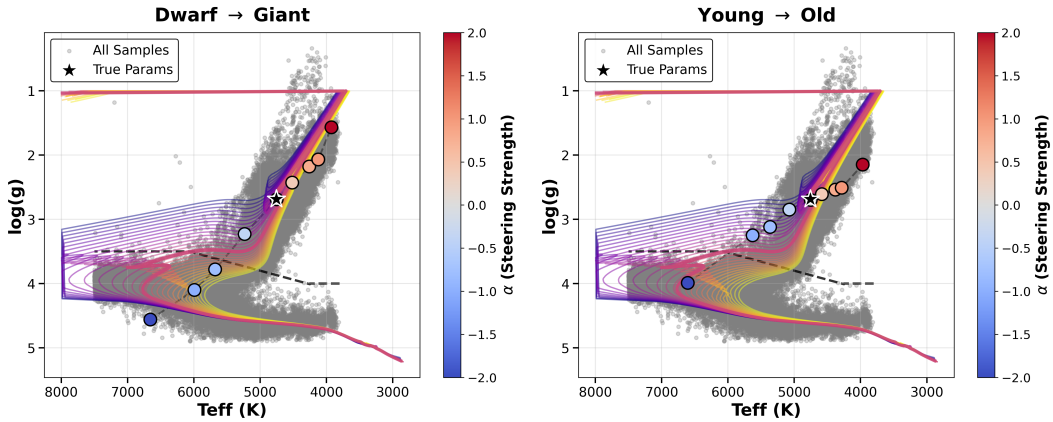


Figure 3: Example of the steering effect for two different concepts - Dwarf to Giants (left) and Young to Old (right). In both panels, the black star represents the true parameters of the star under consideration. The colored circles represent the generated parameters with different α values. The colored lines represent theoretical isochrones - curves with constant age. The dashed black line represents a separation between dwarfs and giants from Ciardi et al. (2011). The background gray points represent the true parameters of the entire sample set.

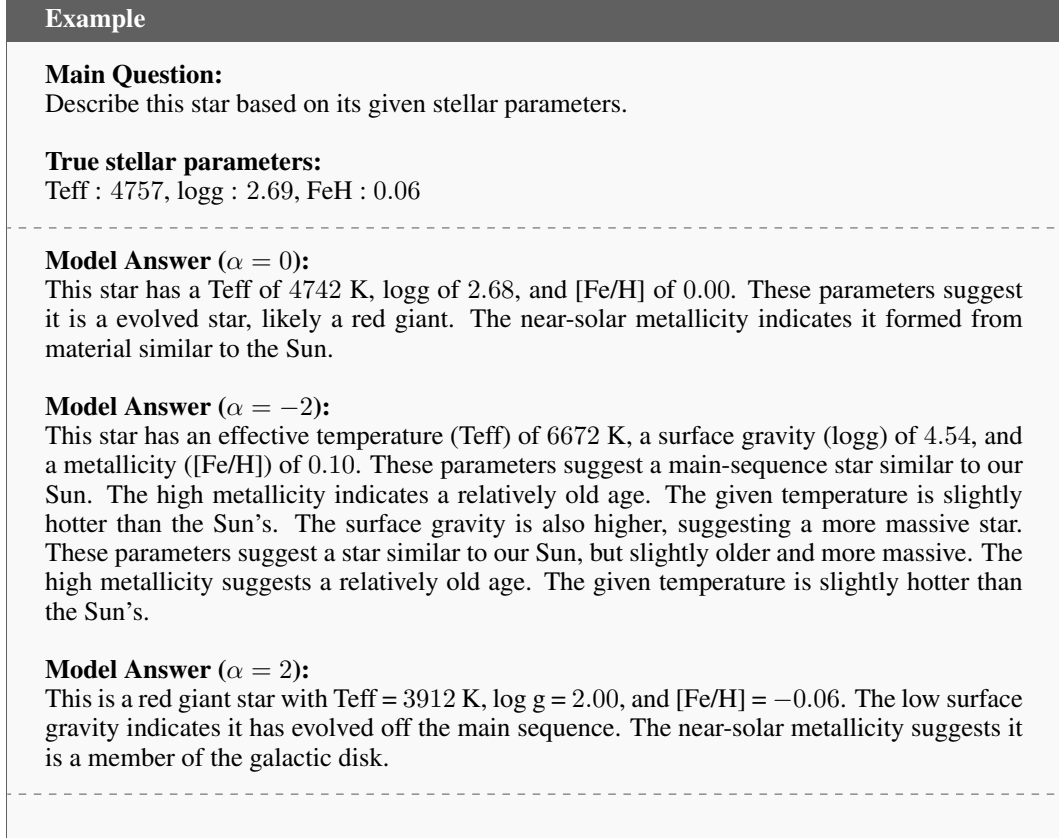


Figure 4: Answers generated by the model during the steering experiment, for the example in Figure 3, left panel, for $\alpha = 0, -2, 2$

intuitive, this conclusion should be taken with caution as the features come from two different models, and might have other subtle differences. Therefore, to conclusively attribute the performance differences to sparsity, additional experiments are needed. However, the striking performance gap, which was not observed in MLP regression during SC and SViT training, suggests that architectural choices in the feature encoder significantly affect the LLM’s ability to interpret latent representations.

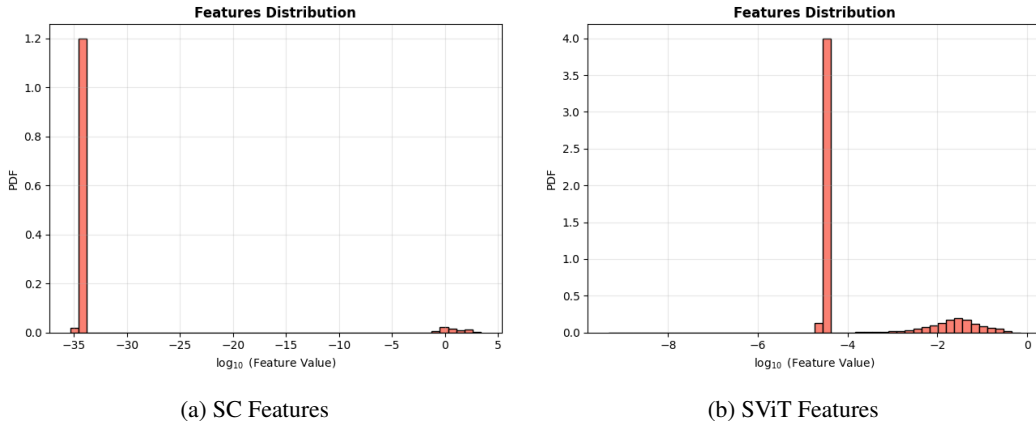


Figure 5: Distributions of latent feature values for SC (left) and SViT (right) models.

Table 3: Performance comparison for T_{eff} , $\log g$ and metallicity (Fe/H). All values were extracted from the models’ answers.

Model	T_{eff} [K]		$\log g$ [dex]		[Fe/H] [dex]	
	MAE ↓	RMSE ↓	MAE ↓	RMSE ↓	MAE ↓	RMSE ↓
LI-Llama-8B-SC	26.50	63.96	0.04	0.11	0.03	0.06
LI-Llama-8B-SViT	161.92	638.44	0.38	0.76	0.25	0.42

5.4 INTERPRETABILITY OF LATENT SPACE

The previous experiment is encouraging, as it highlights a subtle difference between latent features that is not easily identified with standard tools. Indeed, both spectra models achieved comparable performance during their training. Yet, the difference in the ability of the LLM to interpret the features implies a significant difference between them. This difference can be seen when looking at concept directions, like in section 5.2. To test the characteristic of the concept direction, we project features from the test set on the direction vectors. We then classify the projections according to the same physical criteria that were used to create the concept and compare the populations. This is a way to measure whether opposite concepts (for example ‘hot star’ vs ‘cool star’) have distinct features. Figure 6 shows that the sparse features (from the SC model) result in distinct separation between concepts, while the dense features (from the SViT model) result in more mixed concepts. This difference can be qualitatively measured using the Kolmogorov-Smirnov test, which tests the hypothesis that two populations are drawn from the same distribution. Table 4 shows that in the sparse feature space, opposite concepts present two clearly separated distributions ($p\text{-value} < 10^{-85}$), and in the dense feature space, the separation is not always significant ($p\text{-value} \sim 10^{-1}$ for $\log g$ and FeH). This analysis suggests that the concepts in the sparse feature space are likely more linearly separable compared to the dense alternative. Our model naturally highlighted this fact with the poor performance of the LLM using dense features. This suggests that our model can serve as an effective *latent interpreter*, and that it is possible to probe the latent space using LLM. Of course, interpretability using performance analysis is not ideal, and more effective methods should be investigated. However, the fact that we see such a performance gap implies that such methods are possible.

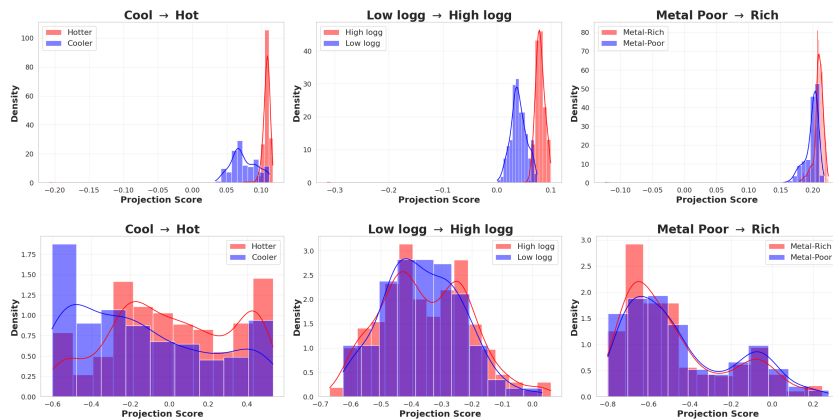


Figure 6: Projections of latent features from the test set on concepts from the training set. The upper row corresponds to SC features, and the lower row corresponds to SViT features.

Table 4: \log_{10} of the p-value of a Kolmogorov-Smirnov test for the hypothesis that projections of features on two distinct concepts are drawn from the same distribution. Lower values mean a lower probability that this hypothesis is true.

Model	$\log_{10}(\text{p-value}) - T_{\text{eff}}$	$\log_{10}(\text{p-value}) - \log g$	$\log_{10}(\text{p-value}) - \text{FeH}$
LI-Llama-8B-Sparse	-135.2	-154.4	-85.6
LI-Llama-8B-Dense	-10.3	-0.86	-1.1

6 DISCUSSION

In this work, we presented *Latent Interpreter*—a framework for aligning scientific foundation models with large language models, using stellar astrophysics as a case study. Our results demonstrate that a lightweight adapter network, combined with low-rank adaptation (LoRA), can effectively translate high-dimensional physical latent spaces into the semantic space of an LLM.

Our main results are as follows: first, we show that by combining latent features information, general physics understanding of the LLM, and the ability to provide the LLM additional information easily, our model can solve complex scientific tasks (e.g., predict the mass of the star given its radius), that are not feasible for spectra-only or text-only models. We also show that this ability scales with LLM size. Second, the steering experiments in Section 5.2 provide compelling evidence that the model learns the *topology* of the physical parameter space, not just statistical correlations. The ability to smoothly traverse the latent space along physically meaningful axes suggests that the adapter preserves the continuous nature of physical laws when mapping to the discrete token space. Lastly, we showed that using two different scientific features with different topologies (sparse vs. dense features) results in a significant performance gap of the LLM, which demonstrates the ability of using LLMs as sophisticated interpretability machines for scientific latent space.

Limitations and Future Work. This paper serves as a proof of concept. As such, relatively small LLMs and a simple unimodal spectra model were used. To fully utilize the potential of this approach, larger LLMs and scientific foundation models should be used. In addition, our approach relies on a ‘Teacher-Student’ distillation pipeline. While effective, the student model is fundamentally bounded by the quality and biases of the teacher’s synthetic descriptions. Furthermore, our current architecture is unidirectional: it can describe data but cannot generate scientific data from text. Enabling such a bidirectional flow requires a different architecture, which is a focus of future work.

REFERENCES

Josh Abramson, Jonas Adler, Jack Dunger, Richard Evans, Tim Green, Alexander Pritzel, Olaf Ronneberger, Lindsay Willmore, Andrew J. Ballard, Joshua Bambrick, Sebastian W. Bodenstein, David A. Evans, Chia-Chun Hung, Michael O'Neill, David Reiman, Kathryn Tunyasuvunakool, Zachary Wu, Akvilė Žemgulytė, Eirini Arvaniti, Charles Beattie, Ottavia Bertolli, Alex Bridgland, Alexey Cherepanov, Miles Congreve, Alexander I. Cowen-Rivers, Andrew Cowie, Michael Figurnov, Fabian B. Fuchs, Hannah Gladman, Rishabh Jain, Yousuf A. Khan, Caroline M. R. Low, Kuba Perlin, Anna Potapenko, Pascal Savy, Sukhdeep Singh, Adrian Stecula, Ashok Thillaisundaram, Catherine Tong, Sergei Yakneen, Ellen D. Zhong, Michal Zielinski, Augustin Žídek, Victor Bapst, Pushmeet Kohli, Max Jaderberg, Demis Hassabis, and John M. Jumper. Accurate structure prediction of biomolecular interactions with AlphaFold 3. *Nature*, 630(8016):493–500, 2024. ISSN 1476-4687. doi: 10.1038/s41586-024-07487-w. URL <https://doi.org/10.1038/s41586-024-07487-w>.

Rio Alexa Fear, Payel Mukhopadhyay, Michael McCabe, Alberto Bietti, and Miles Cranmer. Physics Steering: Causal Control of Cross-Domain Concepts in a Physics Foundation Model. *arXiv e-prints*, art. arXiv:2511.20798, November 2025. doi: 10.48550/arXiv.2511.20798.

Lei Bai, Zhongrui Cai, Yuhang Cao, Maosong Cao, Weihan Cao, Chiyu Chen, Haojiong Chen, Kai Chen, Pengcheng Chen, Ying Chen, Yongkang Chen, Yu Cheng, Pei Chu, Tao Chu, Erfei Cui, Ganqu Cui, Long Cui, Ziyun Cui, Nianchen Deng, Ning Ding, Nanqing Dong, Peijie Dong, Shihan Dou, Sinan Du, Haodong Duan, Caihua Fan, Ben Gao, Changjiang Gao, Jianfei Gao, Songyang Gao, Yang Gao, Zhangwei Gao, Jiaye Ge, Qiming Ge, Lixin Gu, Yuzhe Gu, Aijia Guo, Qipeng Guo, Xu Guo, Conghui He, Junjun He, Yili Hong, Siyuan Hou, Caiyu Hu, Hanglei Hu, Jucheng Hu, Ming Hu, Zhouqi Hua, Haian Huang, Junhao Huang, Xu Huang, Zixian Huang, Zhe Jiang, Lingkai Kong, Linyang Li, Peiji Li, Pengze Li, Shuaibin Li, Tianbin Li, Wei Li, Yuqiang Li, Dahua Lin, Junyao Lin, Tianyi Lin, Zhishan Lin, Hongwei Liu, Jiangning Liu, Jiayao Liu, Junnan Liu, Kai Liu, Kaiwen Liu, Kuikun Liu, Shichun Liu, Shudong Liu, Wei Liu, Xinyao Liu, Yuhong Liu, Zhan Liu, Yinquan Lu, Haijun Lv, Hongxia Lv, Huijie Lv, Qitan Lv, Ying Lv, Chengqi Lyu, Chenglong Ma, Jianpeng Ma, Ren Ma, Runmin Ma, Runyuan Ma, Xinzhu Ma, Yichuan Ma, Zihan Ma, Sixuan Mi, Junzhi Ning, Wenchang Ning, Xinle Pang, Jiahui Peng, Runyu Peng, Yu Qiao, Jiantao Qiu, Xiaoye Qu, Yuan Qu, Yuchen Ren, Fukai Shang, Wenqi Shao, Junhao Shen, Shuaike Shen, Chunfeng Song, Demin Song, Diping Song, Chenlin Su, Weijie Su, Weigao Sun, Yu Sun, Qian Tan, Cheng Tang, Huanze Tang, Kexian Tang, Shixiang Tang, Jian Tong, Aoran Wang, Bin Wang, Dong Wang, Lintao Wang, Rui Wang, Weiyun Wang, Wenhai Wang, Jiaqi Wang, Yi Wang, Ziyi Wang, Ling-I Wu, Wen Wu, Yue Wu, Zijian Wu, Linchen Xiao, Shuhao Xing, Chao Xu, Huihui Xu, Jun Xu, Ruiliang Xu, Wanghan Xu, GanLin Yang, Yuming Yang, Haochen Ye, Jin Ye, Shenglong Ye, Jia Yu, Jiashuo Yu, Jing Yu, Fei Yuan, Yuhang Zang, Bo Zhang, Chao Zhang, Chen Zhang, Hongjie Zhang, Jin Zhang, Qiaosheng Zhang, Qiuyinzhe Zhang, Songyang Zhang, Taolin Zhang, Wenlong Zhang, Wenwei Zhang, Yechen Zhang, Ziyang Zhang, Haiteng Zhao, Qian Zhao, Xiangyu Zhao, Xiangyu Zhao, Bowen Zhou, Dongzhan Zhou, Peiheng Zhou, Yuhao Zhou, Yunhua Zhou, Dongsheng Zhu, Lin Zhu, and Yicheng Zou. Intern-S1: A Scientific Multimodal Foundation Model. *arXiv e-prints*, art. arXiv:2508.15763, August 2025. doi: 10.48550/arXiv.2508.15763.

Jai Bardhan, Radhikesh Agrawal, Abhiram Tilak, Cyrin Neeraj, and Subhadip Mitra. HEP-JEPA: A foundation model for collider physics using joint embedding predictive architecture. *arXiv e-prints*, art. arXiv:2502.03933, February 2025. doi: 10.48550/arXiv.2502.03933.

Travis A. Berger, Daniel Huber, Jennifer L. van Saders, Eric Gaidos, Jamie Tayar, and Adam L. Kraus. The Gaia-Kepler Stellar Properties Catalog. I. Homogeneous Fundamental Properties for 186,301 Kepler Stars. *Astronomical Journal*, 159(6):280, June 2020. doi: 10.3847/1538-3881/159/6/280.

Cristian Bodnar, Wessel P. Bruinsma, Ana Lucic, Megan Stanley, Anna Allen, Johannes Brandstetter, Patrick Garvan, Maik Riechert, Jonathan A. Weyn, Haiyu Dong, Jayesh K. Gupta, Kit Thambiratnam, Alexander T. Archibald, Chun-Chieh Wu, Elizabeth Heider, Max Welling, Richard E. Turner, and Paris Perdikaris. A foundation model for the Earth system. *Nature*, 641(8065):1180–1187, May 2025. ISSN 1476-4687. doi: 10.1038/s41586-025-09005-y. URL <https://doi.org/10.1038/s41586-025-09005-y>.

Lucas Carrit Delgado Pinheiro, Ziru Chen, Bruno Caixeta Piazza, Ness Shroff, Yingbin Liang, Yuan-Sen Ting, and Huan Sun. Large Language Models Achieve Gold Medal Performance at the International Olympiad on Astronomy & Astrophysics (IOAA). *arXiv e-prints*, art. arXiv:2510.05016, October 2025. doi: 10.48550/arXiv.2510.05016.

Anoop Cherian, Radu Corcodel, Siddarth Jain, and Diego Romeres. LLMPH: Complex Physical Reasoning Using Large Language Models and World Models. *arXiv e-prints*, art. arXiv:2411.08027, November 2024. doi: 10.48550/arXiv.2411.08027.

David R. Ciardi, Kaspar von Braun, Geoff Bryden, Julian van Eyken, Steve B. Howell, Stephen R. Kane, Peter Plavchan, Solange V. Ramírez, and John R. Stauffer. Characterizing the Variability of Stars with Early-release Kepler Data. *Astronomical Journal*, 141(4):108, April 2011. doi: 10.1088/0004-6256/141/4/108.

Tijmen de Haan, Yuan-Sen Ting, Tirthankar Ghosal, Tuan Dung Nguyen, Alberto Accomazzi, Azton Wells, Nesar Ramachandra, Rui Pan, and Zechang Sun. Achieving GPT-4o level performance in astronomy with a specialized 8B-parameter large language model. *Scientific Reports*, 15(1):13751, April 2025. doi: 10.1038/s41598-025-97131-y.

Steffen Eger, Yong Cao, Jennifer D’Souza, Andreas Geiger, Christian Greisinger, Stephanie Gross, Yufang Hou, Brigitte Krenn, Anne Lauscher, Yizhi Li, Chenghua Lin, Nafise Sadat Moosavi, Wei Zhao, and Tristan Miller. Transforming Science with Large Language Models: A Survey on AI-assisted Scientific Discovery, Experimentation, Content Generation, and Evaluation. *arXiv e-prints*, art. arXiv:2502.05151, February 2025. doi: 10.48550/arXiv.2502.05151.

Euclid Collaboration, M. Siudek, M. Huertas-Company, M. Smith, G. Martinez-Solaeche, F. Lanusse, S. Ho, E. Angeloudi, P. A. C. Cunha, H. Domínguez Sánchez, M. Dunn, Y. Fu, P. Iglesias-Navarro, J. Junais, J. H. Knapen, B. Laloux, M. Mezcua, W. Roster, G. Stevens, J. Vega-Ferrero, N. Aghanim, B. Altieri, A. Amara, S. Andreon, N. Auricchio, H. Aussel, C. Bacigalupi, M. Baldi, S. Bardelli, P. Battaglia, A. Biviano, A. Bonchi, E. Branchini, M. Brescia, J. Brinchmann, S. Camera, G. Cañas-Herrera, V. Capobianco, C. Carbone, J. Carretero, S. Casas, F. J. Castander, M. Castellano, G. Castignani, S. Cavuoti, K. C. Chambers, A. Cimatti, C. Colodro-Conde, G. Congedo, C. J. Conselice, L. Conversi, Y. Copin, F. Courbin, H. M. Courtois, M. Cropper, A. Da Silva, H. Degaudenzi, G. De Lucia, A. M. Di Giorgio, J. Dinis, C. Dolding, H. Dole, F. Dubath, C. A. J. Duncan, X. Dupac, S. Dusini, S. Escoffier, M. Farina, R. Farinelli, F. Faustini, S. Ferriol, F. Finelli, S. Fotopoulou, M. Frailis, E. Franceschi, S. Galeotta, K. George, B. Gillis, C. Giocoli, J. Gracia-Carpio, B. R. Granett, A. Grazian, F. Grupp, S. Gwyn, S. V. H. Haugan, W. Holmes, I. M. Hook, F. Hormuth, A. Hornstrup, K. Jahnke, M. Jhabvala, E. Keihänen, S. Kermiche, A. Kiessling, B. Kubik, M. Kümmel, M. Kunz, H. Kurki-Suonio, Q. Le Boulc’h, A. M. C. Le Brun, D. Le Mignant, S. Ligori, P. B. Lilje, V. Lindholm, I. Lloro, G. Mainetti, D. Maino, E. Maiorano, O. Mansutti, S. Marcin, O. Marggraf, M. Martinelli, N. Martinet, F. Marulli, R. Massey, S. Maurogordato, H. J. McCracken, E. Medinaceli, S. Mei, M. Melchior, Y. Mellier, M. Meneghetti, E. Merlin, G. Meylan, A. Mora, M. Moresco, L. Moscardini, R. Nakajima, C. Neissner, S. M. Niemi, J. W. Nightingale, C. Padilla, S. Paltani, F. Pasian, K. Pedersen, W. J. Percival, V. Pettorino, S. Pires, G. Polenta, M. Poncet, L. A. Popa, L. Pozzetti, F. Raison, A. Renzi, J. Rhodes, G. Riccio, E. Romelli, M. Roncarelli, R. Saglia, Z. Sakr, A. G. Sánchez, D. Sapone, B. Sartoris, J. A. Schewtschenko, P. Schneider, T. Schrabback, M. Scodégio, A. Secroun, G. Seidel, M. Seiffert, S. Serrano, P. Simon, C. Sirignano, G. Sirri, L. Stanco, J. Steinwagner, P. Tallada-Crespí, A. N. Taylor, I. Tereno, S. Toft, R. Toledo-Moreo, F. Torradeflot, I. Tutasaus, L. Valenziano, J. Valiviita, T. Vassallo, G. Verdoes Kleijn, A. Veropalumbo, Y. Wang, J. Weller, A. Zacchei, G. Zamorani, F. M. Zerbi, I. A. Zinchenko, E. Zucca, V. Allevato, M. Ballardini, M. Bolzonella, E. Bozzo, C. Burigana, R. Cabanac, A. Cappi, D. Di Ferdinando, J. A. Escartin Vigo, L. Gabarra, J. Martín-Fleitas, S. Matthew, N. Mauri, R. B. Metcalf, and A. Pezzotta. Euclid Quick Data Release (Q1) Exploring galaxy properties with a multi-modal foundation model. *arXiv e-prints*, art. arXiv:2503.15312, March 2025. doi: 10.48550/arXiv.2503.15312.

Anmol Gulati, James Qin, Chung-Cheng Chiu, Niki Parmar, Yu Zhang, Jiahui Yu, Wei Han, Shibo Wang, Zhengdong Zhang, Yonghui Wu, and Ruoming Pang. Conformer: Convolution-augmented Transformer for Speech Recognition. *arXiv e-prints*, art. arXiv:2005.08100, May 2020. doi: 10.48550/arXiv.2005.08100.

Thomas Hayes, Roshan Rao, Halil Akin, Nicholas J. Sofroniew, Deniz Oktay, Zeming Lin, Robert Verkuil, Vincent Q. Tran, Jonathan Deaton, Marius Wiggert, Rohil Badkundri, Irhum Shafkat, Jun Gong, Alexander Derry, Raul S. Molina, Neil Thomas, Yousuf A. Khan, Chetan Mishra, Carolyn Kim, Liam J. Bartie, Matthew Nemeth, Patrick D. Hsu, Tom Sercu, Salvatore Candido, and Alexander Rives. Simulating 500 million years of evolution with a language model. *Science*, 387(6736):850–858, 2025. doi: 10.1126/science.ads0018. URL <https://www.science.org/doi/10.1126/science.ads0018>.

Dan Hendrycks and Kevin Gimpel. Gaussian Error Linear Units (GELUs). *arXiv e-prints*, art. arXiv:1606.08415, June 2016. doi: 10.48550/arXiv.1606.08415.

Edward J. Hu, Yelong Shen, Phillip Wallis, Zeyuan Allen-Zhu, Yuanzhi Li, Shean Wang, Lu Wang, and Weizhu Chen. LoRA: Low-Rank Adaptation of Large Language Models. *arXiv e-prints*, art. arXiv:2106.09685, June 2021. doi: 10.48550/arXiv.2106.09685.

Ming Hu, Chenglong Ma, Wei Li, Wanghan Xu, Jiamin Wu, Jucheng Hu, Tianbin Li, Guohang Zhuang, Jiaqi Liu, Yingzhou Lu, Ying Chen, Chaoyang Zhang, Cheng Tan, Jie Ying, Guocheng Wu, Shujian Gao, Pengcheng Chen, Jiashi Lin, Haitao Wu, Lulu Chen, Fengxiang Wang, Yuanyuan Zhang, Xiangyu Zhao, Feilong Tang, Encheng Su, Junzhi Ning, Xinyao Liu, Ye Du, Changkai Ji, Pengfei Jiang, Cheng Tang, Ziyan Huang, Jiayao Liu, Jiaqi Wei, Yuejin Yang, Xiang Zhang, Guangshuai Wang, Yue Yang, Huihui Xu, Ziyang Chen, Yizhou Wang, Chen Tang, Jianyu Wu, Yuchen Ren, Siyuan Yan, Zhonghua Wang, Zhongxing Xu, Shiyan Su, Shangquan Sun, Runkai Zhao, Zhisheng Zhang, Dingkang Yang, Jinjie Wei, Jiaqi Wang, Jiahao Xu, Jiangtao Yan, Wenhao Tang, Hongze Zhu, Yu Liu, Fudi Wang, Yiqing Shen, Yuanfeng Ji, Yanzhou Su, Tong Xie, Hongming Shan, Chun-Mei Feng, Zhi Hou, Diping Song, Lihao Liu, Yanyan Huang, Lequan Yu, Bin Fu, Shujun Wang, Xiaomeng Li, Xiaowei Hu, Yun Gu, Ben Fei, Benyou Wang, Yuewen Cao, Minjie Shen, Jie Xu, Haodong Duan, Fang Yan, Hongxia Hao, Jielan Li, Jiajun Du, Yanbo Wang, Imran Razzak, Zhongying Deng, Chi Zhang, Lijun Wu, Conghui He, Zhao-hui Lu, Jinhai Huang, Wenqi Shao, Yihao Liu, Siqi Luo, Yi Xin, Xiaohong Liu, Fenghua Ling, Yuqiang Li, Aoran Wang, Siqi Sun, Qihao Zheng, Nanqing Dong, Tianfan Fu, Dongzhan Zhou, Yan Lu, Wenlong Zhang, Jin Ye, Jianfei Cai, Yirong Chen, Wanli Ouyang, Yu Qiao, Zongyuan Ge, Shixiang Tang, Junjun He, Chunfeng Song, Lei Bai, and Bowen Zhou. A Survey of Scientific Large Language Models: From Data Foundations to Agent Frontiers. *arXiv e-prints*, art. arXiv:2508.21148, August 2025. doi: 10.48550/arXiv.2508.21148.

Ilay Kamai, Alex M. Bronstein, and Hagai B. Perets. Machine-learning inference of stellar properties using integrated photometric and spectroscopic data. *arXiv e-prints*, art. arXiv:2507.10666, July 2025. doi: 10.48550/arXiv.2507.10666.

Nolan Koblischke, Liam Parker, Francois Lanusse, Irina Espejo Morales, Jo Bovy, and Shirley Ho. Semantic search for 100M+ galaxy images using AI-generated captions. *arXiv e-prints*, art. arXiv:2512.11982, December 2025. doi: 10.48550/arXiv.2512.11982.

Henry W. Leung and Jo Bovy. Towards an astronomical foundation model for stars with a transformer-based model. *MNRAS*, 527(1):1494–1520, January 2024. doi: 10.1093/mnras/stad3015.

Ilya Loshchilov and Frank Hutter. Decoupled Weight Decay Regularization. *arXiv e-prints*, art. arXiv:1711.05101, November 2017. doi: 10.48550/arXiv.1711.05101.

Siddharth Mishra-Sharma, Yiding Song, and Jesse Thaler. PAPERCLIP: Associating Astronomical Observations and Natural Language with Multi-Modal Models. *arXiv e-prints*, art. arXiv:2403.08851, March 2024. doi: 10.48550/arXiv.2403.08851.

Liam Parker, Francois Lanusse, Jeff Shen, Ollie Liu, Tom Hehir, Leopoldo Sarra, Lucas Meyer, Micah Bowles, Sebastian Wagner-Carena, Helen Qu, Siavash Golkar, Alberto Bietti, Hatim Bourfoune, Nathan Casserau, Pierre Cornette, Keiya Hirashima, Geraud Krawezik, Ruben Ohana, Nicholas Lourie, Michael McCabe, Rudy Morel, Payel Mukhopadhyay, Mariel Pettee, Bruno Regaldo-Saint Blanchard, Kyunghyun Cho, Miles Cranmer, and Shirley Ho. AION-1: Omnimodal Foundation Model for Astronomical Sciences. *arXiv e-prints*, art. arXiv:2510.17960, October 2025.

Roussel Rahman and Aashwin Ananda Mishra. A Fragile Number Sense: Probing the Elemental Limits of Numerical Reasoning in LLMs. *arXiv e-prints*, art. arXiv:2509.06332, September 2025. doi: 10.48550/arXiv.2509.06332.

Michael J. Smith, Ryan J. Roberts, Eirini Angeloudi, and Marc Huertas-Company. AstroPT: Scaling Large Observation Models for Astronomy. *arXiv e-prints*, art. arXiv:2405.14930, May 2024. doi: 10.48550/arXiv.2405.14930.

Kyle Swanson, Wesley Wu, Nash L. Bulaong, John E. Pak, and James Zou. The Virtual Lab of AI agents designs new SARS-CoV-2 nanobodies. *Nature*, 646(8085):716–723, October 2025. ISSN 1476-4687. doi: 10.1038/s41586-025-09442-9. URL <https://doi.org/10.1038/s41586-025-09442-9>.

Guy Tennenholz, Yinlam Chow, Chih-Wei Hsu, Jihwan Jeong, Lior Shani, Azamat Tulepbergenov, Deepak Ramachandran, Martin Mladenov, and Craig Boutilier. Demystifying Embedding Spaces using Large Language Models. *arXiv e-prints*, art. arXiv:2310.04475, October 2023. doi: 10.48550/arXiv.2310.04475.

Francisco Villaescusa-Navarro, Boris Bolliet, Pablo Villanueva-Domingo, Adrian E. Bayer, Aidan Acquaah, Chetana Amancharla, Almog Barzilay-Siegal, Pablo Bermejo, Camille Bilodeau, Pablo Cárdenas Ramírez, Miles Cranmer, Urbano L. França, ChangHoon Hahn, Yan-Fei Jiang, Raul Jimenez, Jun-Young Lee, Antonio Lerario, Osman Mamun, Thomas Meier, Anupam A. Ojha, Pavlos Protopapas, Shimanto Roy, David N. Spergel, Pedro Tarancón-Álvarez, Ujjwal Tiwari, Matteo Viel, Digvijay Wadekar, Chi Wang, Bonny Y. Wang, Licong Xu, Yossi Yovel, Shuwen Yue, Wen-Han Zhou, Qiyao Zhu, Jiajun Zou, and Iñigo Zubeldia. The Denario project: Deep knowledge AI agents for scientific discovery. *arXiv e-prints*, art. arXiv:2510.26887, October 2025. doi: 10.48550/arXiv.2510.26887.

Chun Wang, Yang Huang, Haibo Yuan, Huawei Zhang, Maosheng Xiang, and Xiaowei Liu. The Value-added Catalog for LAMOST DR8 Low-resolution Spectra. *The Astrophysical Journal Supplement Series*, 259(2):51, April 2022. doi: 10.3847/1538-4365/ac4df7.

Yue Wu, Bing Du, Ali Luo, Yongheng Zhao, and Hailong Yuan. Automatic stellar spectral parameterization pipeline for LAMOST survey. In Alan Heavens, Jean-Luc Starck, and Alberto Krone-Martins (eds.), *Statistical Challenges in 21st Century Cosmology*, volume 306 of *IAU Symposium*, pp. 340–342, May 2014. doi: 10.1017/S1743921314010825.

Tong Xie, Yuwei Wan, Wei Huang, Zhenyu Yin, Yixuan Liu, Shaozhou Wang, Qingyuan Linghu, Chunyu Kit, Clara Grazian, Wenjie Zhang, Imran Razzak, and Bram Hoex. DARWIN Series: Domain Specific Large Language Models for Natural Science. *arXiv e-prints*, art. arXiv:2308.13565, August 2023. doi: 10.48550/arXiv.2308.13565.

Sharaf Zaman, Michael J. Smith, Pranav Khetarpal, Rishabh Chakrabarty, Michele Ginolfi, Marc Huertas-Company, Maja Jabłońska, Sandor Kruk, Matthieu Le Lain, Sergio José Rodríguez Méndez, and Dimitrios Tanoglidis. AstroLLaVA: towards the unification of astronomical data and natural language. *arXiv e-prints*, art. arXiv:2504.08583, April 2025. doi: 10.48550/arXiv.2504.08583.

Gang Zhao, Yong-Heng Zhao, Yao-Quan Chu, Yi-Peng Jing, and Li-Cai Deng. LAMOST spectral survey — An overview. *Research in Astronomy and Astrophysics*, 12(7):723–734, July 2012. doi: 10.1088/1674-4527/12/7/002.

Zhenzhen Zhuang, Jiandong Chen, Hongfeng Xu, Yuwen Jiang, and Jialiang Lin. Large language models for automated scholarly paper review: A survey. *arXiv e-prints*, art. arXiv:2501.10326, January 2025. doi: 10.48550/arXiv.2501.10326.

A APPENDIX

A.1 IMPLEMENTATION DETAILS

The raw spectra were taken from LAMOST DR8 (Zhao et al., 2012; Wang et al., 2022). In all models, we used 8 effective tokens for the features. For the Adapter Network, we used a 2-layer

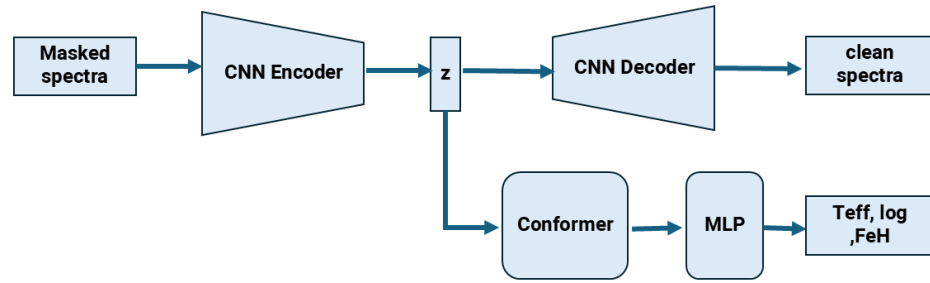
MLP with a hidden dimension of 512 and a GELU activation function (Hendrycks & Gimpel, 2016). For LoRA fine-tuning, we used a rank of 8 and $\alpha = 8$. We used an AdamW optimizer (Loshchilov & Hutter, 2017) with a learning rate of 10^{-4} and a scheduler that performs a linear warmup followed by cosine decay. Training was done in two steps - we first trained only the AN, and then applied LoRA with the AN frozen. We set the number of epochs in the first step to 5. The convergence of LoRA typically occurs within several additional epochs. All models were trained using 4 L40s or 4 H200 GPUs for a maximum of 30 epochs.

A.2 CONCEPTS CRITERION

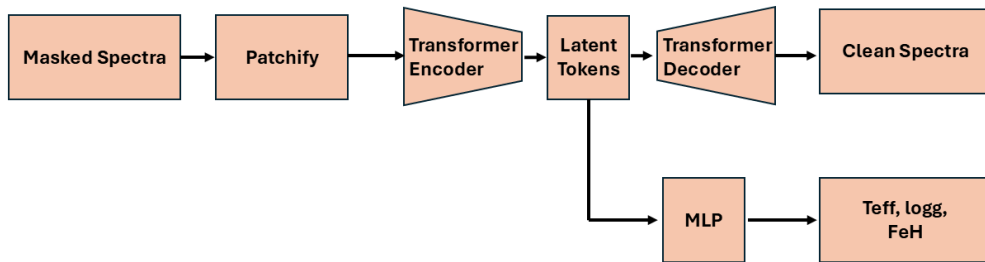
Concept	Criteria
Cool \rightarrow Hot	$T_{\text{eff}} > 6250$ (Hot), $T_{\text{eff}} < 4500$ (Cool)
Low $\log g$ \rightarrow High $\log g$	$\log g > 4.5$ (High), $\log g < 3.0$ (Low)
Metal Poor \rightarrow Metal Rich	$[\text{Fe}/\text{H}] > 0.2$ (Rich), $[\text{Fe}/\text{H}] < -0.2$ (Poor)
Dwarf \rightarrow Giant	$\log g < \text{Thresh}(T_{\text{eff}})$ (Giant), $\log g \geq \text{Thresh}(T_{\text{eff}})$ (Dwarf)
Low Mass \rightarrow High Mass	Top 25% vs. Bottom 25% (controlled for Age & $[\text{Fe}/\text{H}]$)
Young \rightarrow Old	Top 25% vs. Bottom 25% (controlled for Mass & $[\text{Fe}/\text{H}]$)

Table 5: Criteria used to define the concept directions. For the evolution concept, $\text{Thresh}(T_{\text{eff}})$ was taken from Ciardi et al. (2011). For Mass and Age, data is stratified into local bins of determining parameters (e.g., Age bins of 1 Gyr, Mass bins of $0.1 M_{\odot}$) to isolate the concept.

A.3 ADDITIONAL FIGURES



(a) Spectral Conformer (SC)



(b) Spectral ViT (SViT)

Figure 7: Diagrams of the spectra models used in this work.

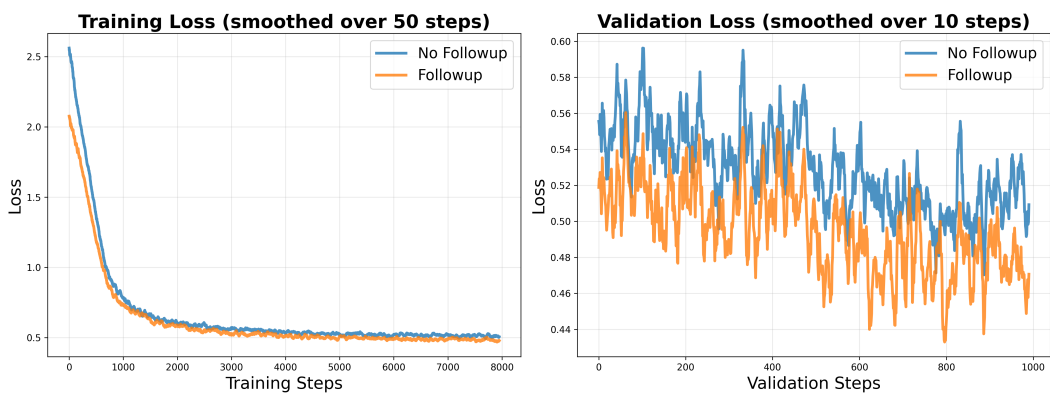


Figure 8: Effect of followup questions on training and validation loss

Example

General prompt:

You are an expert Stellar Astrophysicist. You are provided with: 1. A visual plot of a stellar spectrum. 2. A raw data summary consisting of two arrays: Wavelength (Angstroms) and Flux (normalized).

Your Goal: precise inference of physical parameters.

OUTPUT FORMAT: Return ONLY valid JSON.

```
{"spectral type": "string (e.g. G2V)", "teff pred": "integer (Kelvin)", "logg pred": "float", "feh pred": "float (dex)", "confidence score": "float (0-1)", "key lines detected": ["list", "of", "lines"], "reasoning trace": "Brief physics explanation of why you chose these values."}
```

Additional Knowledge Base for Spectral Analysis: <*Spectra Guidelines*> Use this knowledge to inform your analysis.

Sample question:

Here are the wavelength and flux data arrays for Star ID 154001001: <*Wavelength and Flux Values*>

Analyze the spectrum.

Gemini-3 pro Answer:

spectral type: G2V

T_{eff} : 5750

$logg$: 4.45

FeH : -0.1

confidence score: 0.95

key lines detected: ['Ca II K (3933 Å)', 'Ca II H (3968 Å)', 'H-delta (4101 Å)', 'G-band (4300 Å)', 'H-gamma (4340 Å)', 'H-beta (4861 Å)', 'Mg b (5172 Å)', 'Na D (5890 Å)', 'H-alpha (6563 Å)']

Reasoning trace: The spectrum exhibits the textbook morphology of a solar-type G dwarf. The most prominent features are the deep Ca II H & K absorption lines (3933/3968 Å), which drive the significant break in the continuum around 4000 Å. The distinct absorption of the G-band (CH molecule) at 4300 Å is a primary classifier for G-type stars. The Hydrogen Balmer series (H-alpha, H-beta, H-gamma) is clearly visible but moderate in strength; they are weaker than in F-types and stronger than in K-types, constraining Teff to approximately 5600-5900 K. The Mg b triplet at 5172 Å is visible, and the continuum shape lacks the extreme molecular blanketing of M dwarfs or the blue slope of OB stars. The general 'roughness' of the blue continuum indicates a metallicity consistent with the solar neighborhood ($[Fe/H] = 0$)

True parameters

spectral type: F5

T_{eff} : 6510

$logg$: 4.17

FeH : -0.05

Figure 9: An example of the prompt and answer of Gemini-3 pro zero-shot experiment

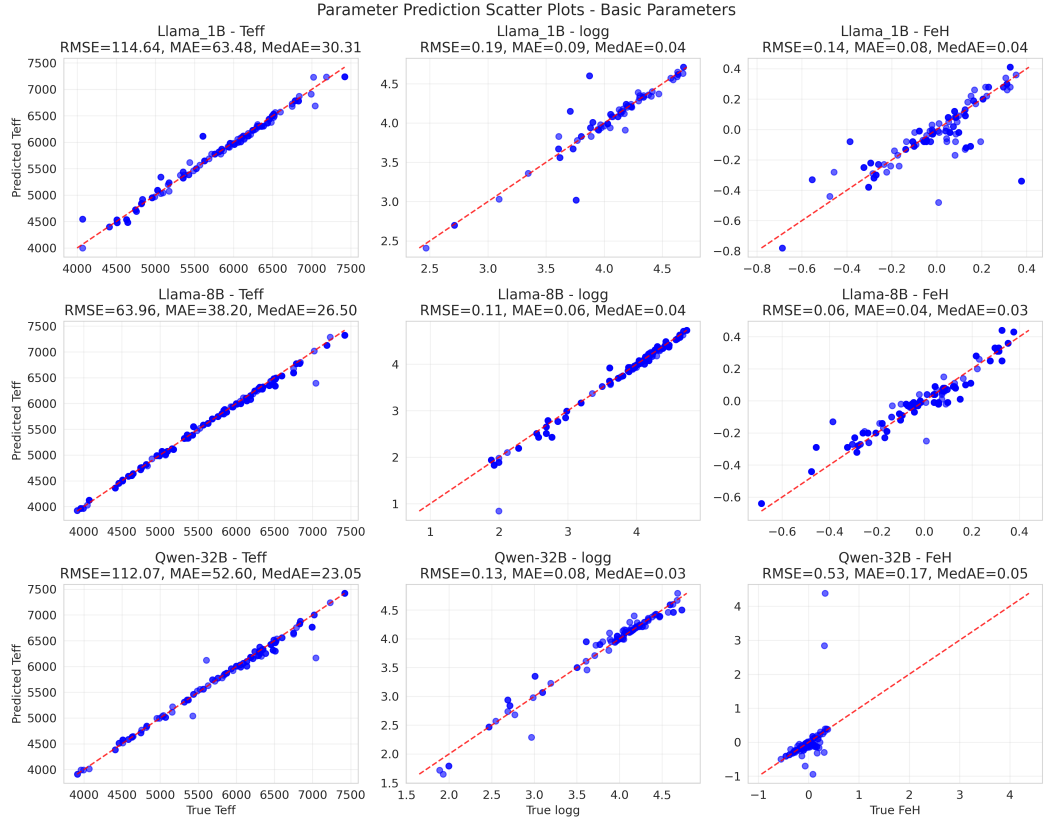


Figure 10: scatter plots of parameter predictions for different models. The columns corresponds to T_{eff} , $logg$, and FeH . The rows correspond to 1B, 8B, and 32B models.

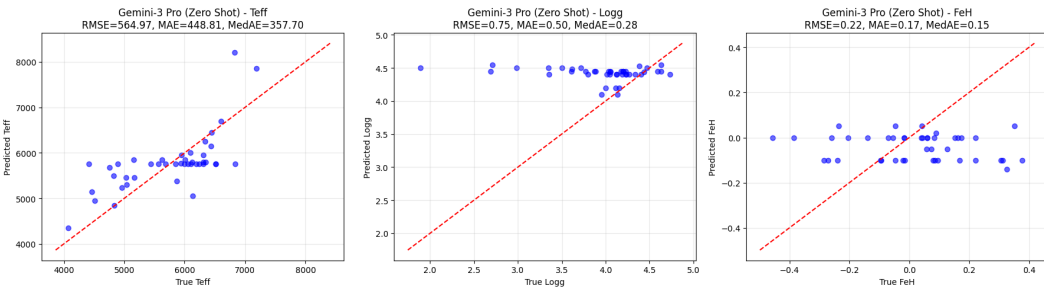


Figure 11: Scatter plots of T_{eff} , $logg$, and FeH for Gemini 3 pro without training (zero shot).

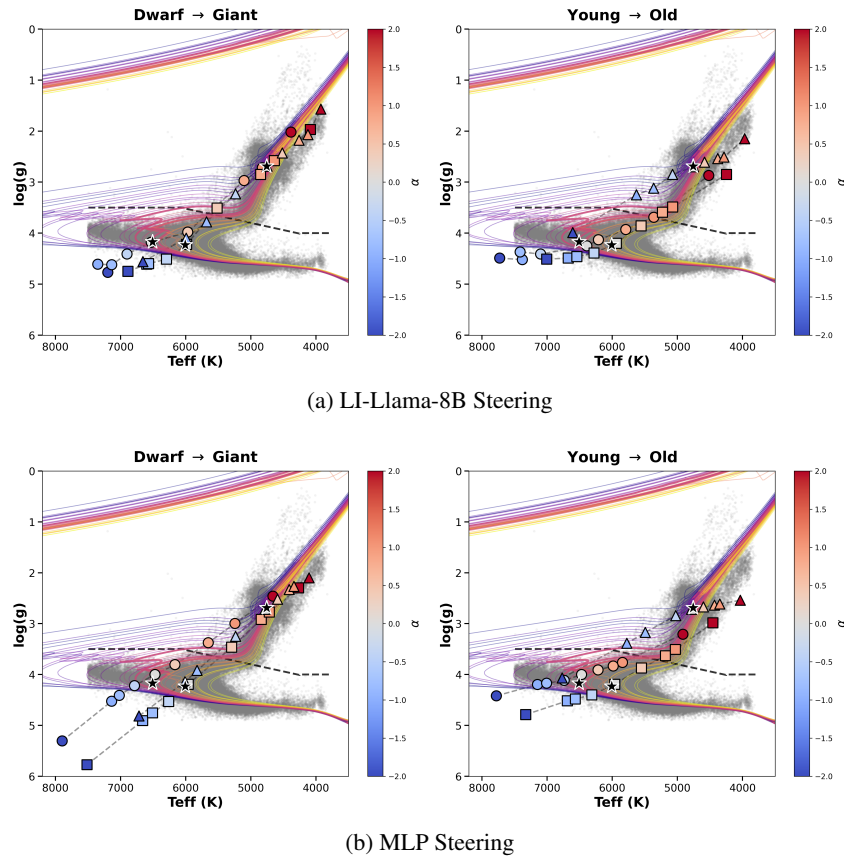


Figure 12: Three steering trajectory examples. The upper panel (a) shows our model, and the lower panel (b) shows an MLP trained to predict stellar parameters. Markers (circles, squares, triangles) represent distinct samples. Note that the MLP trajectories frequently enter non-physical regions, whereas our model remains within physically consistent bounds.

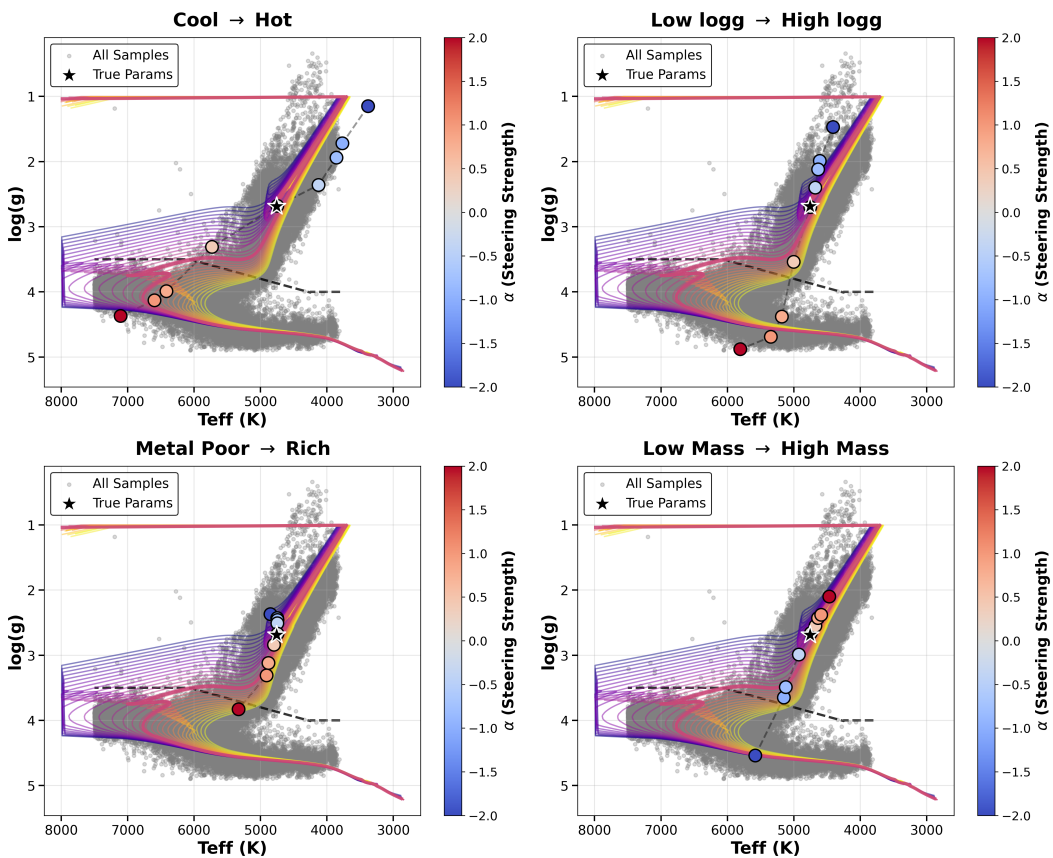


Figure 13: Steering diagrams for the same example as in Figure 3, and additional concepts.